Applied Catalysis B: Environmental 126 (2012) 208–214

Contents lists available at SciVerse ScienceDirect

Applied Catalysis B: Environmental

journal homepage: www.elsevier.com/locate/apcatb

# Novel synthesis of N-doped porous carbons from collagen for electrocatalytic production of $H_2O_2$

Ying-Hui Lee [a], Feng Li [b], Kuo-Hsin Chang [a], Chi-Chang Hu [a,*], Takeo Ohsaka [b,**]

[a] Department of Chemical Engineering, National Tsing Hua University, Hsin-Chu 30013, Taiwan
[b] Department of Electronic Chemistry, Tokyo Institute of Technology, Kanagawa 226-8503, Japan

ARTICLE INFO

*Article history:*
Received 14 October 2011
Received in revised form 16 June 2012
Accepted 26 June 2012
Available online 8 July 2012

*Keywords:*
Carbons
Nitrogen-doping
Collagen
$H_2O_2$ generation
Oxygen reduction

ABSTRACT

Highly porous N-doped carbons for the electrocatalytic production of $H_2O_2$ via oxygen reduction were synthesized from paraformaldehyde cross-linked collagen through heating in vacuum at different temperatures (400–800 °C). SEM images and $N_2$ adsorption/desorption isotherms of such collagen-derived carbons reveal the formation of a sheet-like porous structure with increasing the carbonization temperature. A higher carbonization temperature favors the formation of a quaternary-N structure and the removal of oxygen-containing functional groups and therefore enhances the graphitic crystallinity, which were confirmed by X-ray photoelectron spectroscopy (XPS) and Raman spectroscopy. The collagen-derived carbon synthesized at 800 °C for 6 h shows a good electrocatalytic activity for the four-electron oxygen reduction reaction (ORR). On the other hand, the carbons prepared at 400–800 °C for 4 h possess a high selectivity for the $H_2O_2$ production at potentials more negative than 0.6 V. The $H_2O_2$ production percentage for the carbon synthesized at 400 °C even reached 93%. In comparison with undoped carbons, the much more positive onset potentials and the nearly two-electron process of the ORR on these collagen-derived porous carbons reveal their unique electrocatalytic activity for $H_2O_2$ production.


## 1. Introduction

Recently, many research efforts focus on the synthesis and characterization of porous carbon materials doped with nitrogen in various forms because of their promising applications in several electrochemical systems, such as electrode materials of supercapacitors [1–6] and biosensors [7–9] as well as electrocatalysts to facilitate the oxygen reduction reaction (ORR) [10–12]. The utilization of N-doped porous carbon materials to catalyze the ORR is of great interest since traditionally used platinum nanoparticles are very expensive and hard to disperse homogeneously [13] without considering the poisoning issue caused by, for example, carbon monoxide [14]. Therefore, various N-doped carbon materials, such as N-doped porous carbons [15–17], N-doped carbon nanofibers [18], N-doped carbon nanotubes (CNTs) [10,19–23] and N-doped graphene [11,24–26] have been developed and demonstrated to exhibit the catalytic activity toward the ORR as a suitable replacement for platinum.

According to previous research, the catalytic activity of N-doped carbon materials for the ORR arises from the active sites on N-doped structures such as pyridinic-N and quaternary-N [15–17,19,22–24,27,28], and these unique active sites are considered to promote the four-electron reduction of oxygen, similar to that of Pt catalysts [15,16,19,20,25]. However, it has been also reported that N-doped structures do not actually contribute to the four-electron reduction of oxygen, but to a mixed reaction of two-electron and four-electron reduction paths [18,21,29]. Accordingly, the number of electrons involved in the ORR and its reaction paths on various N-doped carbon materials are worthy being investigated and are of high interest to electrochemists and catalyst researchers.

In general, there are two strategies for synthesizing N-doped carbon materials. Due to the well-established carbonization and graphitization technologies, porous carbons in various forms can be chemically doped with nitrogen through ammoxidation [3,30–32]. The most promising advantage of this post-treatment method is the effective control in porosity, nanostructures, and pore size distribution while the N-doping efficiency is low and diverse [31,32]. The other strategy is to synthesize porous carbons through direct carbonization of an N-containing precursor [1,4,5,33]. The merit of this strategy is the possibility in enhancing the N-doping content and varying the N-doping structure although the resultant porosity and pore size are hard to be controlled. In our previous work [34], a simple method to synthesize carbon nanosheets doped with nitrogen through carbonization of collagen was proposed while detailed

* Corresponding author. Tel.: +886 3 5736027; fax: +886 3 5736027.
** Corresponding author at: Department of Electronic Chemistry, Interdisciplinary Graduate School of Science and Engineering, Tokyo Institute of Technology, G1-5 4259 Nagatsuta, Midori-ku, Yokohama-Shi 226-8502, Japan. Tel.: +81 045 924 5404.
*E-mail addresses:* cchu@che.nthu.edu.tw (C.-C. Hu), ohsaka.t.aa@m.titech.ac.jp (T. Ohsaka).

0926-3373/$ – see front matter © 2012 Elsevier B.V. All rights reserved.
http://dx.doi.org/10.1016/j.apcatb.2012.06.031

evaluation and comparison of various synthesis parameters have not been done.

Based on the above understanding and viewpoints, collagen, the most abundant protein in mammals, [35,36] is employed to prepare carbon materials with the intention of obtaining N-doped structures derived from the amino groups in collagen as well as to control the porosity. In consistence with our previous work [34], the collagen-derived carbon (synthesized at 800 °C for 6 h) shows a good electrocatalytic activity toward the four-electron ORR. On the other hand, those obtained at the carbonization temperatures from 400 to 800 °C for 4 h are demonstrated to possess a high electrocatalytic activity for the two-electron ORR to effectively produce $H_2O_2$. This unique property of being able to accomplish the two-electron ORR over a wide potential range demonstrates that collagen-derived carbons are excellent electrocatalysts for in situ generation of $H_2O_2$. In fact, such in situ $H_2O_2$ generation with high selectivity has been proposed by using a fuel-cell system [37,38], which is believed to be promising for removing organic pollutants in waste water [39–44] and etching Ti and TiW layers in the flip-chip technology for microchip packaging and high level system assembly. In fact, several carbon materials, such surface modified carbon-PTFE [45,46], Printex L6 [39], active carbon [42,47], and reticulated vitreous carbon [40,41,48], have been reported to exhibit high efficiency for the $H_2O_2$ generation. In this work, 93% $H_2O_2$ production can be obtained from the collagen-derived carbons simply by the carbonization of the precursor without any further treatments. The unique two-electron ORR over a wide potential range and the high production efficiency of $H_2O_2$ show the promising application potential of these collagen-derived carbons.

## 2. Experimental

### 2.1. Preparation of carbon materials

Collagen gels were prepared by the similar procedure to that mentioned in our previous work [34]. These as-prepared gels were heated in vacuum at a rate of 4 °C $min^{-1}$ to 400, 600 and 800 °C, respectively, and held at these temperatures for 4 h. These samples are denoted as CG400, CG600 and CG800, respectively. The one carbonized at 800 °C for 6 h ([34]) is denoted as CG800-6.

### 2.2. Material characterization of carbon materials

X-ray photoelectron spectroscopy (XPS) measurement was performed on a Kratos Axis Ultra DLD (Kratos analytical, USA) which employed Al monochromator ($h\nu$ = 1486.69 eV) irradiation as the photosource. The SEM images of collagen-derived carbons were obtained by Hitachi S-4700I (Hitachi, Japan). Raman spectra were recorded on Lab RAM HR (Horoba, France) equipped with a HeNe laser source (wavelength: 633 nm). $N_2$ adsorption/desorption (BET) analysis was performed at 77 K using a NOVA 4200*e* (Quantachrome®, USA), equipped with an automated surface area and pore size analyzer. Before the BET analysis, samples were degassed at 200 °C for 5 h.

### 2.3. Electrochemical analysis

The electrochemical catalytic activities of collagen-derived carbons for the ORR were investigated using a rotating ring-disk electrode (RRDE) voltammetry (Pine Research Instrumentation, USA). Suspensions of carbon samples were prepared by adding 5 wt% Nafion® (E.I. du Pont de Nemours & Co., USA) and 99.5% ethanol (Kanto Chemical Co. Inc., Japan) for CG400, CG600 and CG800-6 or 5 wt% Nafion® and N-methyl-2-pyrrolidone for CG800 in the volume ratio of 1:15. The homogeneous suspensions were coated on the glassy-carbon (GC) electrode for RRDE voltammetry with the loading mass of 1 mg $cm^{-2}$. For comparison purposes, the ORR activities of commercial Pt/C (20%, E-TEK, USA) and single walled carbon nanotubes (SWCNT, Sigma–Aldrich, USA) which was pretreated by a highly concentrated $H_2SO_4$–$HNO_3$ mixture (in the volume ratio of 3:1) have been investigated. The suspensions were also prepared by mixing 5 wt% Nafion® and ethanol in a volume ratio of 1:15. The mass loading of Pt/C (20%) and SWCNT on the GC electrode were also 1 mg $cm^{-2}$.

## 3. Results and discussion

### 3.1. Morphology and porosity

The morphologies of collagen-derived carbons were examined by SEM images and the typical results are shown in Fig. 1. CG400 generally shows a dense but rough morphology. A comparison of these SEM images demonstrates that with increasing the carbonization temperature, these carbons become more porous and sheet-like. The appearance of the sheet-like morphology for CG800 and CG800-6 is consistent with our previous results [34]. The sheet-like morphology is attributed to the cross-linking of collagen with paraformaldehyde since collagen-derived carbons prepared at 800 °C did not show such a unique microstructure when the collagen gel was not cross-linked with paraformaldehyde (data not shown here).

The porous properties of collagen-derived carbons can be further confirmed by the $N_2$ adsorption/desorption isotherms, as shown in Fig. 2. Also the BET surface area and the pore volume data are summarized in Table 1. For CG400, the hysteresis loop at relative pressure ($P/P_0$) higher than 0.3 is not clear and the intercept for volume occupied due to $N_2$ adsorption is approximately equal to 0. These results indicate the ineffective generation of pores, leading to a small surface area for CG400. When the carbonization temperature is 600 °C, the hysteresis loop of $N_2$ adsorption/desorption isotherms is very clear, which reveals the significant formation of mesopores although the intercept for volume occupied due to $N_2$ adsorption is not significantly changed in comparison with CG400. For CG800 and CG800-6, the intercepts for volume occupied due to $N_2$ adsorption are 27.4 and 167.4 cc $g^{-1}$, respectively. The difference indicates that significant amount of micropores available for $N_2$ adsorption can be exposed by prolonging the carbonization time. The shape of all the hysteresis loops confirms the existence of slit-like mesopores [49,50], which agrees well with the sheet-like morphology observed in the SEM images. All the above results indicate that the size of mesopores is mainly determined by the carbonization temperature and time. Accordingly, due to the appearance of more micropores by increasing the carbonization temperature and by prolonging the carbonization time to 6 h, the specific surface area of CG800-6 is the highest among the carbons prepared in this study, which reaches 681.4 $m^2$ $g^{-1}$.

### 3.2. The degree of N-doping and graphitic crystallinity

CG800-6, as the same material as in our previous study [34], has been reported to possess N-doped structures due to the presence of abundant amino groups in collagen. This was confirmed again by examining the XPS core-level spectra of N 1s for CG 400, CG600, CG800 and CG800-6. In general, there are four N-doped structures in such carbons: pyridinic-N (398.5 eV), pyrrolic-N (400 eV), quaternary-N (401.2 eV), and pyridine-N-oxide (403 eV) [2,5,6], as shown in Fig. 3. The N-doping level varies with the carbonization temperature. Based on Fig. 3, the total content of nitrogen and the amounts of their individual N-doped structures are summarized in Table 2. From the examination of Fig. 3 and Table 2,

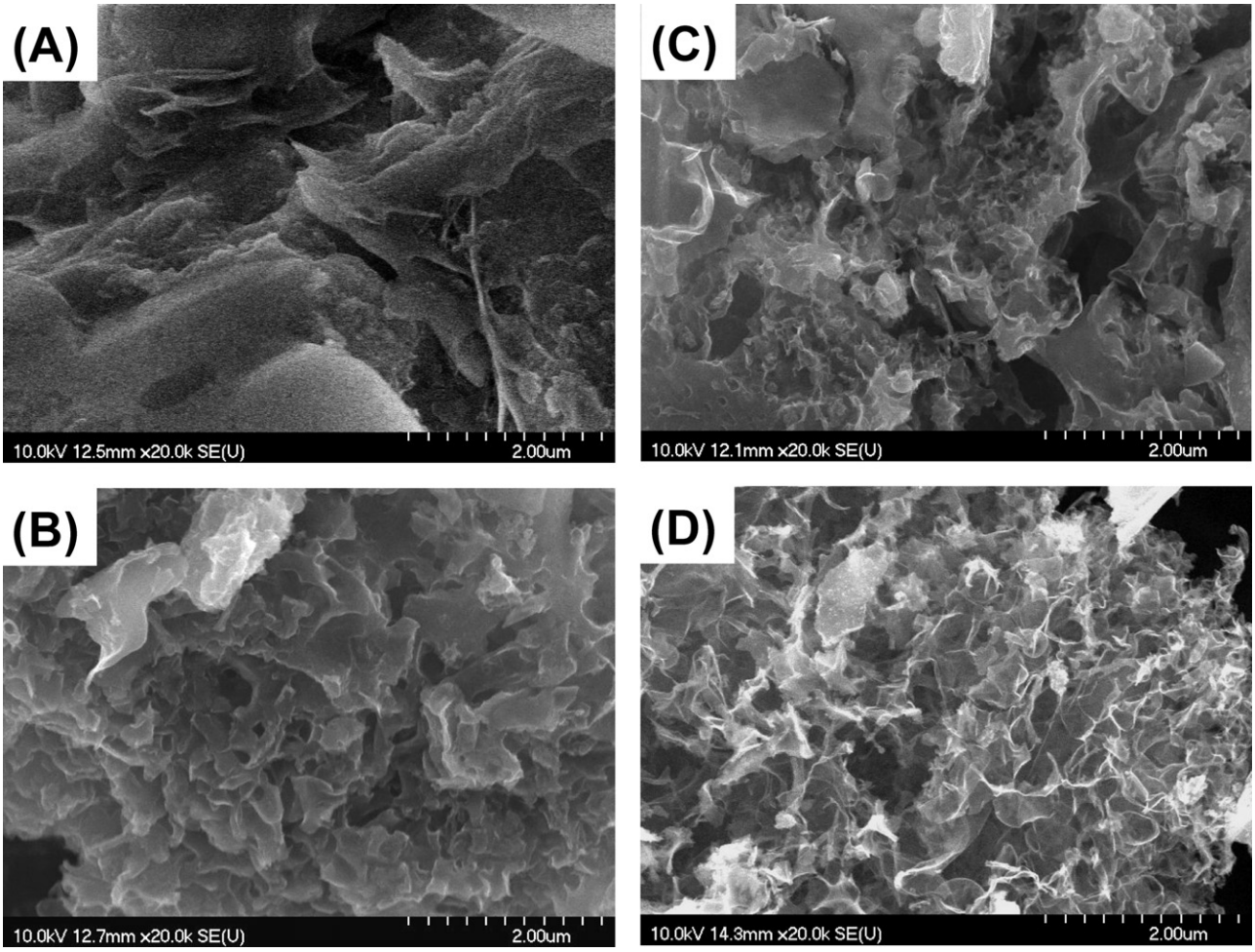


**Fig. 1.** SEM images of (A) CG400, (B) CG600, (C) CG800 and (D) CG800-6.

several features are observed. First, the total content of nitrogen in collagen-derived carbons decreases with increasing the carbonization temperature. This effect in turn results in the gradual loss of all types of N-doped structures in the carbons. Second, considering the relatively unstable nitrogen atoms of pyridinic-N and pyrrolic-N which appear on the edge of graphene, these nitrogen atoms are either removed or surrounded by adjacent carbon atoms to form the more stable quaternary-N at higher carbonization temperatures. Therefore, the amounts of pyridinic-N and pyrrolic-N decrease significantly, especially for the carbonization temperatures above 600 °C, while the amount of quaternary-N remains almost the same. Third, since abundant carboxyl groups are also present in the collagen, surface oxygen-containing functional groups are visible in all the XPS spectra (data are summarized in Table 2). Because these oxygen-containing functional groups are more susceptible to thermal removal, the content of oxygen rapidly decreases as the carbonization temperature increases.

**Table 1**
Data of the BET surface area and pore volume derived from the $N_2$ adsorption/desorption isotherms of CG400, CG600, CG800 and CG800-6.

| | $S_{BET}$ ($m^2\,g^{-1}$) | Intercept at *Y* axis ($cc\,g^{-1}$) | Mesopore volume ($cc\,g^{-1}$) | Micropore volume ($cc\,g^{-1}$) |
|---|---|---|---|---|
| CG400 | 12 | 0.5 | 0.04 | 0 |
| CG600 | 34 | 1.3 | 0.18 | 0 |
| CG800 | 128 | 27.4 | 0.24 | 0.04 |
| CG800-6 | 681 | 167.4 | 0.32 | 0.3 |

Besides the N-doping level, the graphitic crystallinity of collagen-derived carbons was also investigated by means of Raman spectroscopy. Fig. 4 shows that for these four collagen-derived carbons, D and G bands are observed around 1355 $cm^{-1}$ and 1580 $cm^{-1}$, respectively [51]. The appearance of D band

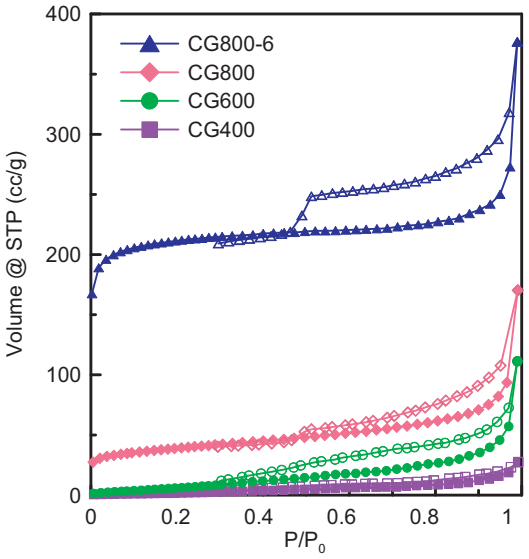


**Fig. 2.** $N_2$ adsorption/desorption isotherms of CG400, CG600, CG800 and CG800-6.

**Table 2**
Deconvolution results (at%) for the XPS core-level spectra of N 1s and O 1s for four collagen-derived carbons.

| | N (at%) | N-6 | N-5 | N—Q | N—X | O (at%) | C—O | C=O | O—C=O |
|---|---|---|---|---|---|---|---|---|---|
| CG400 | 6 | 2.7 | 2.6 | 0.7 | 0 | 18.3 | 7.1 | 7.9 | 3.3 |
| CG600 | 5 | 2.2 | 1.1 | 1.5 | 0.2 | 15.7 | 7.7 | 6.1 | 1.9 |
| CG800 | 2.3 | 0.7 | 0.4 | 1.0 | 0.2 | 8.4 | 1.5 | 5.5 | 1.0 |
| CG800-6 | 1.8 | 0.4 | 0.3 | 1.0 | 0.1 | 8.5 | 1.9 | 5.6 | 1.0 |

demonstrates that disordered graphitic structures and edge defects exist in these N-doped porous carbons [52]. CG400 shows broad D and G bands with a low intensity, indicating the poor graphitic crystallinity in this carbon matrix when collagen was carbonized at 400 °C. However, a comparison of the four spectra shows that as the carbonization temperature increases, both bands become sharper. The increase in the G band intensity reveals the increase of graphitic structures and the removal of surface oxygen-containing functional groups. The formation of more graphitic structures in small domains, however, also results in the enhancement of graphitic defects formed at the edges of these graphite domains, and therefore contributes to the higher intensity of D band. Hence, both results indicate that the overall graphitic crystallinity of the collagen-derived carbons has been improved at higher carbonization temperatures. To sum up, a higher carbonization temperature not only generates greater porosity but also favors the formation of quaternary-N and graphitic structure in the carbon matrix, thus improving the crystallinity of these N-doped porous carbons. From the material analyses, it is clear that different levels of porosity, N-doping, and graphitic crystallinity can be simply controlled by varying the carbonization temperature and time for the collagen.

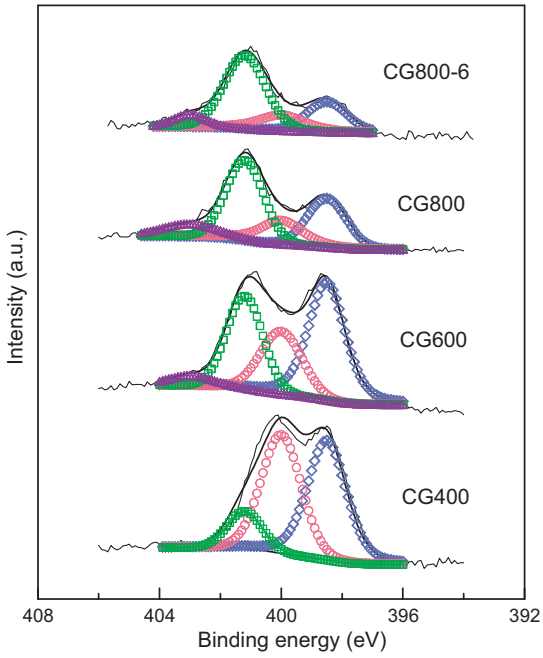


**Fig. 3.** XPS core-level spectra of N 1s for CG400, CG600, CG800 and CG800-6. The black line is the raw spectrum; the symbols ◇, ○, □, and △ correspond to pyridine-N, pyrrolic-N, quaternary-N and pyridine-N-oxide, respectively.

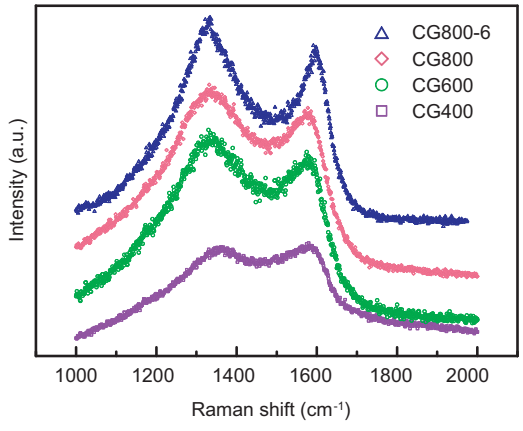


**Fig. 4.** Raman spectra of CG400, CG600, CG800 and CG800-6 obtained at 633 nm excitation.

### 3.3. The RRDE study

Since N-doped carbon materials have been reported to be excellent electrocatalysts for the ORR due to the presence of N-doped structures as active sites [15–17,19,22–24,27,28], the electrocatalytic performances of the present collagen-derived N-doped porous carbons for the ORR were evaluated using the RRDE voltammetry. Fig. 5 shows the voltammograms for the ORR obtained at the GC electrodes coated with CG400, CG600, CG800 and CG800-6. The results for the pretreated SWCNT and the commercial Pt/C (20%) are also shown for a comparison purpose. Clearly, all the collagen-derived N-doped carbons do exhibit electrocatalytic activity for the ORR. The onset potentials of oxygen reduction, which were estimated as a potential at which the current density of 30 μA cm$^{-2}$ was attained, for CG400, CG600, CG800 and CG800-6 are equal to ca. 0.72, 0.80, 0.88 and 0.92 V, respectively. The positive shift of onset potential and an increase in the limiting current of the ORR for N-doped carbons are observed as the carbonization temperature increases, indicating that the greater porosity obtained at a higher carbonization temperature results in the more

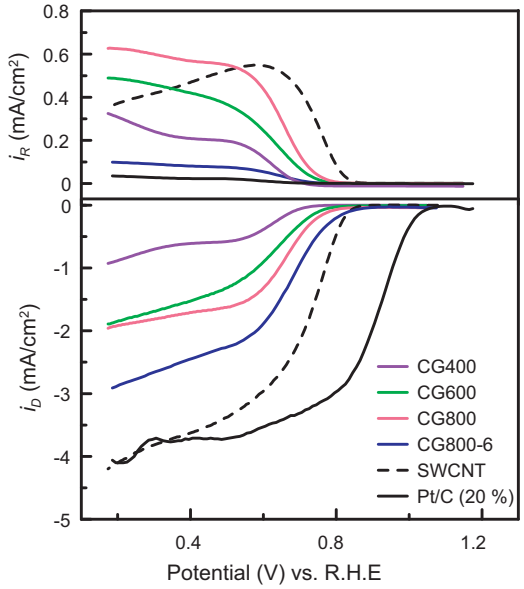


**Fig. 5.** The RRDE voltammograms obtained from the GC disk electrodes coated with CG400, CG600, CG800, CG800-6, Pt/C (20%), and SWCNT in $O_2$-saturated 0.1 M KOH at 5 mV s$^{-1}$ and a rotating speed of 900 rpm.

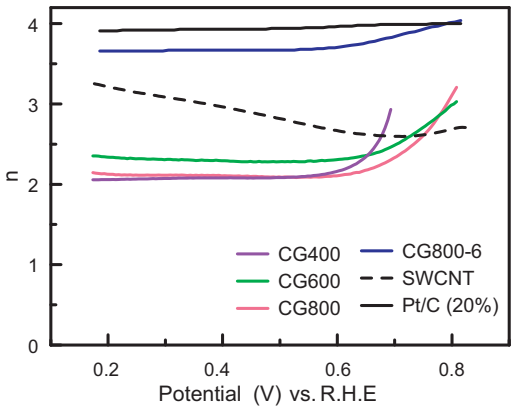


**Fig. 6.** The number of electrons involved in the ORR at the GC electrodes coated with CG400, CG600, CG800, CG800-6, Pt/C (20%), and SWCNT in $O_2$-saturated 0.1 M KOH.

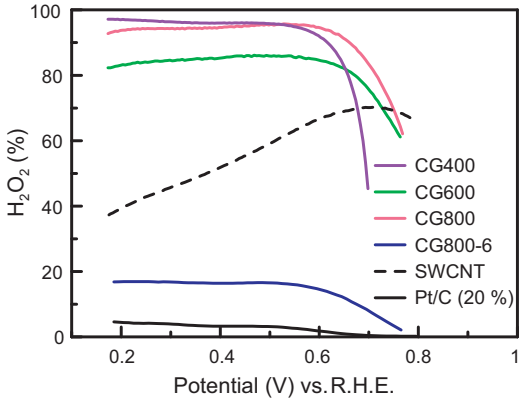


**Fig. 7.** The percentage of $H_2O_2$ formation upon the ORR at the GC electrodes coated with CG400, CG600, CG800, CG800-6, Pt/C (20%), and SWCNT in $O_2$-saturated 0.1 M KOH.

effective exposure of N-doped structures (i.e., active sites such as pyridinic-N and quaternary-N). Interestingly, SWCNT without any N-doped structures also shows the significant current for the ORR and the onset potential is close to that of CG800, i.e., 0.85 V. Compared with CG800-6, a higher current density was observed for SWCNT, probably due to the higher electrolyte-accessible surface area of SWCNT (see below). Note that SWCNT used here was pre-treated with a $H_2SO_4$–$HNO_3$ mixture to generate abundant surface oxygen-containing functional groups which allowed us to prepare a well-dispersed suspension solution and then to obtain a good coating on the GC electrode. The greater hydrophilic degree and the smaller size of pre-treated SWCNT generally result in a larger electrolyte-accessible surface area for the ORR. This statement is supported by estimating the charging current of the electrical double layer, which is proportional to the electrochemically active surface area, that is, the electrolyte-accessible specific surface areas for SWCNT and CG800-6 were estimated to be 678 and 408 $m^2\ g^{-1}$, respectively. Therefore, the relatively larger electrolyte-accessible surface area of SWCNT is considered to result in the higher current density of the ORR in comparison with CG800-6. Similarly, for a series of the collagen-derived N-doped carbons investigated here, greater porosity obtained at a higher carbonization temperature leads to a larger surface area, which in turn offers a facile accessibility of the electrolyte to the active sites of N-doped structures and results in the enhanced current density and the positive shift of the onset potential for the ORR.

In order to gain a further understanding on the electrocatalytic behavior of collagen-derived N-doped carbons for the ORR, the number of electrons involved in the ORR was calculated from the RRDE voltammograms using Eq. (1):

$$n = \frac{4I_D}{I_D + (I_R/N)} \quad (1)$$

where $I_D$, $I_R$ and $N$ represent the disk current, ring current and the collection efficiency of the electrode (0.38) [53], respectively. The obtained values of $n$ are shown as a function of the electrode potential in Fig. 6. Similar to the expensive commercial Pt/C (20%), the $n$ value for CG800-6 is close to 4 (3.7–4), which is in agreement with the values reported for various N-doped carbons [15,16,19,20,25]. This fact together with the positive shift of onset potential to ca. 0.92 V (mentioned previously) suggests that CG800-6 possesses a great potential to serve as the electrocatalyst for the four-electron ORR in the applications of fuel cells and metal-air batteries, which is consistent with the conclusion in our previous work [34]. On the contrary, for CG400, CG600 and CG800, the $n$ values in the potential range of 0.8–0.6 V are potential-dependent and vary from ca. 3 to 2, indicating that the ORR in this potential range takes place actually via both two-electron and four-electron reduction pathways. However, interestingly, at more negative potentials than 0.6 V, the $n$ values for these three N-doped porous carbons are almost independent of the electrode potential and are close to 2, i.e., ca. 2.1, 2.4 and 2.2 for CG400, CG600 and CG800, respectively. Therefore, these collagen-derived carbons are considered as excellent electrocatalysts for the ORR to boost $H_2O_2$ generation. This is also supported by the percentage of $H_2O_2$ formation ($\chi(H_2O_2)$ in %) at these three collagen-derived carbons (Fig. 7), which can be calculated based on Eq. (2):

$$\chi(H_2O_2)\ \text{in}\ \% = \frac{200 \times (I_R/N)}{I_D + (I_R/N)} \quad (2)$$

That is, $\chi(H_2O_2)$ values for CG400, CG600 and CG800 are almost independent of the electrode potential and are equal to 93, 83 and 92%, respectively, demonstrating a high-percentage production of $H_2O_2$ over a wide potential range in comparison with other modified carbons [40,45,46,54] and metal oxide/carbon composites [43,44]. Here it should be noted again that while the electrode materials previously reported for $H_2O_2$ production need tedious surface modification or preparation [40,45,46], the N-doped carbon (CG400) with a low porosity and crystallinity, which can be simply derived from collagen with carbonization at 400 °C, exhibits the $H_2O_2$ production activity as high as 93% for the ORR. Therefore, collagen-derived carbons can be expected as promising electrode materials for the electrogeneration of $H_2O_2$. As for SWCNT, although it exhibits larger current density for the ORR (see Fig. 5), the $n$ value of ca. 3 limits its use as the electrocatalyst for the four-electron ORR. Neither, SWCNT is not a suitable electrocatalyst to boost the electrogeneration of $H_2O_2$ as can be seen from the electrode potential-dependent and lower $\chi(H_2O_2)$ values; i.e., ca. 70–40% in the potential range from ca.0.7 to 0.2 V.

While the ORR current differs among CG400, CG600 and CG800 (Fig. 5), the performance of $H_2O_2$ production is quite similar. This fact implies that the factors determine the production of $H_2O_2$ are distinct from what is necessary for carbon materials to catalyze the four-electron ORR, e.g., the porous structure with a high surface area. Note that a recent study proposed that the presence of surface oxygen-containing functional groups provides hydrophilicity of the carbons and therefore facilitates the production of $H_2O_2$ [39]. This may be also applicable to the present collagen-derived carbons which contain many surface oxygen-containing functional groups owing to the existence of abundant carboxyl groups in collagen. Certain oxygen-containing functional groups such as quinone/hydroquinone have been reported to be effective redox groups to assist in generating $H_2O_2$ [46,55] while it is very hard to isolate the contribution from such functional groups. However, in

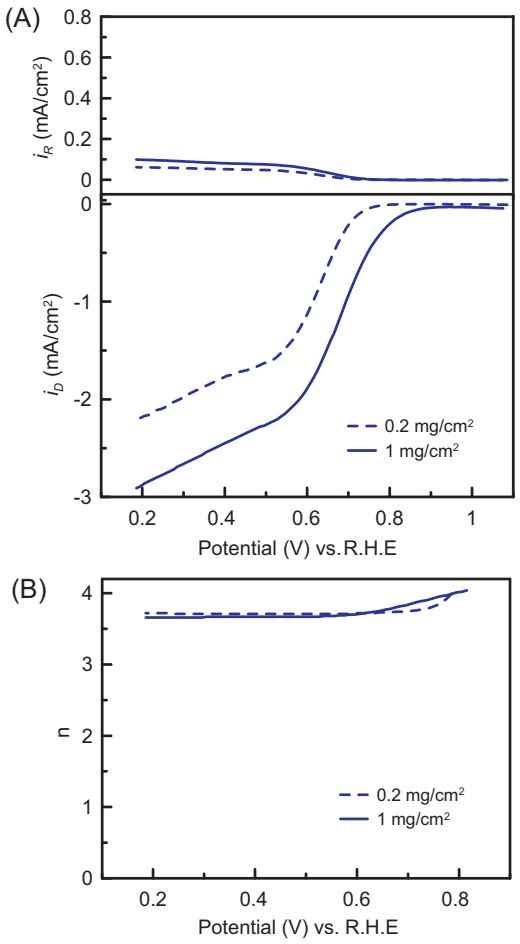


**Fig. 8.** (A) The RRDE voltammograms and (B) the number of electrons involved in the ORR at the GC disk electrode coated with CG800-6 measured in $O_2$-saturated 0.1 M KOH at 5 mV $s^{-1}$ and a rotating speed of 900 rpm (dash line: 0.2 mg $cm^{-2}$, solid line: 1 mg $cm^{-2}$).

comparison with SWCNT which contains abundant surface oxygen-containing functional groups but no N doping, the N-doped carbon structures on CG400, CG600 and CG800 give more positive onset potentials of the ORR for the $H_2O_2$ production (0.88 V, while ca. 0.85 V at SWCNT) and show potential-almost independent *n* values near to 2 (i.e., ca. 2.1, 2.4 and 2.2 on CG400, CG600 and CG800, respectively) in the wide potential range (0.17–0.6 V), revealing the synergistic electrocatalytic effect of combining the N-doped structures and the surface oxygen functional groups on the electrogeneration of $H_2O_2$.

In developing the ORR catalysts of N-doped carbon and Pt/carbon materials for achieving the four-electron reduction purpose, a so-called two-step mechanism (transformation of hydrogen peroxide to water by its further two-electron reduction and/or its catalytic decomposition (disproportionation)) are considered as possible reasons for the increase in *n* with increasing the catalyst loading [56,57]. Accordingly, the casted amount of CG800-6 with *n* close to 4 was changed to examine this effect. Fig. 8A and B respectively show the typical RRDE results and the number of electrons involved in the ORR for CG800-6. Due to the high porosity and the presence of N-doped structures, CG800-6 exhibits superior catalytic activity with *n* close to 4 regardless of the casted amount. Different from the previous study [56] that the catalytic performance of N-doped carbons for the four-electron ORR was reduced with decreasing the casted amount, CG800-6 already exhibits the excellent four-electron ORR catalytic activity at the loading of 0.2 mg $cm^{-2}$ and the decrease in the catalyst loading from 1 to 0.2 mg $cm^{-2}$ makes no significant effects on the transformation of hydrogen peroxide to water. Therefore, unlike CG400, CG600, and CG800 which already demonstrate the excellent two-electron ORR characteristics at 1 mg $cm^{-2}$ catalyst loading, CG800-6 is a desired electrocatalyst for the four-electron ORR in the applications of fuel cells and metal-air batteries.

## 4. Conclusions

N-doped carbons were simply obtained by the carbonization of collagen gels in vacuum. For the collagen-derived carbon which was prepared at 800 °C for 6 h (i.e., CG800-6), the N-doped structures are exposed by the assistance of a highly porous structure to show a good electrocatalytic activity for the four-electron ORR. Contrary to CG800-6, the collagen-derived carbons synthesized at temperatures from 400 to 800 °C for 4 h (i.e., CG400, CG600 and CG800) show the nearly two-electron ORR over a wide potential range of ca. 0.17–0.6 V (vs. RHE), which leads to the potential-almost independent $H_2O_2$ production with the efficiency higher than 80%. The $H_2O_2$ production on CG400 reached as high as 93%, demonstrating that the collagen-derived carbons with N-doped structures but a small surface area possess an excellent selectivity for the $H_2O_2$ production through the ORR. The combination of the N-doped structures and the surface oxygen-containing functional groups on the collagen-derived carbons is believed to generate the synergistic effect for the good selectivity of $H_2O_2$ production.

## Acknowledgement

The financial supports of this work, the National Science Council of ROC-Taiwan under contract no. NSC 98-2221-E-007-078-MY3, 100-2628-E-007-028-MY2, and the boost program from the Low Carbon Energy Research Center of National Tsing Hua University, are gratefully acknowledged.

## References

[1] D. Hulicova, J. Yamashita, Y. Soneda, H. Hatori, M. Kodama, Chemistry of Materials 17 (2005) 1241.
[2] D. Hulicova-Jurcakova, M. Kodama, S. Shiraishi, H. Hatori, Z.H. Zhu, G.Q. Lu, Advanced Functional Materials 18 (2009) 1800.
[3] K.Y. Kang, S.J. Hong, B.I. Lee, J.S. Lee, Electrochemistry Communications 10 (2008) 1105.
[4] Y.J. Kim, Y. Abe, T. Yanagiura, K.C. Park, M. Shimizu, T. Iwazaki, S. Nakagawa, M. Endo, M.S. Dresselhaus, Carbon 45 (2007) 2116.
[5] T.E. Rufford, D. Hulicova-Jurcakova, Z. Zhu, G.Q. Lu, Electrochemistry Communications 10 (2008) 1594.
[6] M. Seredych, D. Hulicova-Jurcakova, G.Q. Lu, T.J. Bandosz, Carbon 46 (2008) 1475.
[7] S. Deng, G. Jian, J. Lei, Z. Hu, H. Ju, Biosensors and Bioelectronics 25 (2009) 373.
[8] Y. Wang, Y. Shao, D.W. Matson, J. Li, Y. Lin, ACS Nano 4 (2010) 1790.
[9] X. Xu, S. Jiang, Z. Hu, S. Liu, ACS Nano 4 (2010) 4292.
[10] N. Alexeyeva, E. Shulga, V. Kisand, I. Kink, K. Tammeveski, Journal of Electroanalytical Chemistry 648 (2010) 169.
[11] D. Geng, Y. Chen, Y. Chen, Y. Li, R. Li, X. Sun, S. Ye, S. Knights, Energy & Environmental Science 4 (2011) 760.
[12] D. Yu, E. Nagelli, F. Du, L. Dai, Journal of Physical Chemistry Letters 1 (2010) 2165.
[13] Z. Peng, H. Yang, Nano Today 4 (2009) 143.
[14] C. Bezerra, L. Zhang, K. Lee, H. Liu, A. Marques, E. Marques, H. Wang, J. Zhang, Electrochimica Acta 53 (2008) 4937.
[15] T. Iwazaki, R. Obinata, W. Sugimoto, Y. Takasu, Electrochemistry Communications 11 (2009) 376.
[16] T. Iwazaki, H. Yang, R. Obinata, W. Sugimoto, Y. Takasu, Journal of Power Sources 195 (2010) 5840.
[17] G. Liu, X. Li, P. Ganesan, B.N. Popov, Applied Catalysis B: Environmental 93 (2009) 156.
[18] S. Maldonado, K.J. Stevenson, Journal of Physical Chemistry B 109 (2005) 4707.
[19] Z. Chen, D. Higgins, H. Tao, R.S. Hsu, Z. Chen, Journal of Physical Chemistry C 113 (2009) 21008.
[20] K. Gong, F. Du, Z. Xia, M. Durstock, L. Dai, Science 323 (2009) 760.

[21] S. Kundu, T.C. Nagaiah, W. Xia, Y. Wang, S. Van Dommele, J.H. Bitter, M. Santa, G. Grundmeier, M. Bron, W. Schuhmann, M. Muhler, Journal of Physical Chemistry C 113 (2009) 14302.
[22] R. Liu, D. Wu, X. Feng, K. Mullen, Angewandte Chemie International Edition 49 (2010) 2565.
[23] C.V. Rao, C.R. Cabrera, Y. Ishikawa, Journal of Physical Chemistry Letters 1 (2010) 2622.
[24] K.R. Lee, K.U. Lee, J.W. Lee, B.T. Ahn, S.I. Woo, Electrochemistry Communications 12 (2010) 1052.
[25] L. Qu, Y. Liu, J.B. Baek, L. Dai, ACS Nano 4 (2010) 1321.
[26] Y. Shao, S. Zhang, M.H. Engelhard, G. Li, G. Shao, Y. Wang, J. Liu, I.A. Aksay, Y. Lin, Journal of Materials Chemistry 20 (2010) 7491.
[27] T. Ikeda, M. Boero, S.F. Huang, K. Terakura, M. Oshima, J.I. Ozaki, Journal of Physical Chemistry C 112 (2008) 14706.
[28] H. Niwa, K. Horiba, Y. Harada, M. Oshima, T. Ikeda, K. Terakura, J.I. Ozaki, S. Miyata, Journal of Power Sources 187 (2009) 93.
[29] Z. Luo, S. Lim, Z. Tian, J. Shang, L. Lai, B. MacDonald, C. Fu, Z. Shen, T. Yu, J. Lin, Journal of Materials Chemistry 21 (2011) 8038.
[30] K. Jurewicz, K. Babel, A. Zí ioï l kowski, H. Wachowska, Electrochimica Acta 48 (2003) 1491.
[31] K. Jurewicz, K. Babeł, A. Ziółkowski, H. Wachowska, Journal of Physics and Chemistry of Solids 65 (2004) 269.
[32] N.D. Kim, W. Kim, J.B. Joo, S. Oh, P. Kim, Y. Kim, J. Yi, Journal of Power Sources 180 (2008) 671.
[33] G. Lota, K. Lota, E. Frackowiak, Electrochemistry Communications 9 (2007) 1828.
[34] Y.H. Lee, Y.F. Lee, K.H. Chang, C.C. Hu, Electrochemistry Communications 13 (2011) 50.
[35] A.D. Covington, Chemical Society Reviews 26 (1997) 111.
[36] K.E. Kadler, D.F. Holmes, J.A. Trotter, J.A. Chapman, Biochemical journal 316 (1996) 1.
[37] K. Otsuka, I. Yamanaka, Electrochimica Acta 35 (1990) 319.
[38] I. Yamanaka, T. Onizawa, S. Takenaka, K. Otsuka, Angewandte Chemie International Edition 42 (2003) 3653.
[39] M.H.M.T. Assumpção, R.F.B. De Souza, D.C. Rascio, J.C.M. Silva, M.L. Calegaro, I. Gaubeur, T.R.L.C. Paixão, P. Hammer, M.R.V. Lanza, M.C. Santos, Carbon 49 (2011) 2842.
[40] S.H. Cho, A. Jang, P.L. Bishop, S.H. Moon, Journal of Hazardous Materials 175 (2010) 253.
[41] C.E. La Rotta H, E. D'Elia, E.P.S. Bon, Electronic Journal of Biotechnology 10 (2007) 24.
[42] A. Wang, J. Qu, J. Ru, H. Liu, J. Ge, Dyes and Pigments 65 (2005) 227.
[43] M.H.M.T. Assumpção, D.C. Rascio, J.P.B. Ladeia, R.F.B. De Souza, E. Teixeira Neto, M.L. Calegaro, R.T.S. Oliveira, I. Gaubeur, M.R.V. Lanza, M.C. Santos, International Journal of Electrochemical Science 6 (2011) 1586.
[44] N. Guillet, L. Roué, S. Marcotte, D. Villers, J.P. Dodelet, N. Chhim, S.T. Vin, Journal of Applied Electrochemistry 36 (2006) 863.
[45] J.C. Forti, J.A. Nunes, M.R.V. Lanza, R. Bertazzoli, Journal of Applied Electrochemistry 37 (2007) 527.
[46] J.C. Forti, R.S. Rocha, M.R.V. Lanza, R. Bertazzoli, Journal of Electroanalytical Chemistry 601 (2007) 63.
[47] L. Xu, H. Zhao, S. Shi, G. Zhang, J. Ni, Dyes and Pigments 77 (2008) 158.
[48] C. Badellino, C.A. Rodrigues, R. Bertazzoli, Journal of Applied Electrochemistry 37 (2007) 451.
[49] S. Kumagai, H. Ishizawa, Y. Aoki, Y. Toida, Chemical Engineering Journal 156 (2010) 270.
[50] Y. Matsuo, Y. Sakai, T. Fukutsuka, Y. Sugie, Carbon 47 (2009) 804.
[51] S. Reich, C. Thomsen, Philosophical Transactions of The Royal Society A-Mathematical Physical and Engineering Sciences 362 (2004) 2271.
[52] A.C. Ferrari, Solid State Communications 143 (2007) 47.
[53] M.S. El-Deab, T. Ohsaka, Journal of the Electrochemical Society 153 (2006) A1365.
[54] E.L. Gyenge, C.W. Oloman, Journal of Applied Electrochemistry 31 (2001) 233.
[55] E.L. Gyenge, C.W. Oloman, Journal of Applied Electrochemistry 33 (2003) 655.
[56] E.J. Biddinger, D.v. Deak, D. Singh, H. Marsh, B. Tan, D.S. Knapke, U.S. Ozkan, Journal of the Electrochemical Society 158 (2011) B402.
[57] M. Inaba, H. Yamada, J. Tokunaga, A. Tasaka, Electrochemical Solid-State Letters 7 (2004) A474.